Available online at www.sciencedirect.com
SCIENCE DIRECT®
ELSEVIER
Ultramicroscopy 98 (2004) 145–150
ultramicroscopy
www.elsevier.com/locate/ultramic

Structural study of new hydrocarbon nano-crystals by energy-filtered electron diffraction

J.S. Wu[a], N. Melcer[b], W.P. Sharp[c], M. O'Keeffe[d], J.C.H. Spence[a,*], O.M. Yaghi[b]

[a] *Department of Physics and Astronomy, Arizona State University, Tempe, AZ 85287-1504, USA*
[b] *Department of Chemistry, Materials Design and Discovery Group, University of Michigan, 930 N. University Ave, Ann Arbor, MI 48109, USA*
[c] *Department of Plant Biology, Arizona State University, Tempe, AZ 85287-1504, USA*
[d] *Department of Chemistry, Arizona State University, Tempe, AZ 85287-1504, USA*

Received 31 December 2002; received in revised form 16 April 2003

Dedicated to Professor Fang-hua Li on the occasion of her 70th birthday.

Abstract

A new brittle hydrocarbon has been successfully synthesized in polycrystalline form, and its crystal structure solved by quantitative electron diffraction. By 3D tilting of the nano-crystals, the lattice type and unit cell parameters were determined. (Triclinic, $a = 6.03$ Å, $b = 6.23$ Å, $c = 13.86$ Å, $\alpha = 87.26^\circ$, $\beta = 106.69^\circ$, and $\gamma = 119.01^\circ$.) Spot diffraction patterns were obtained at -165°C using the Koehler selected-area mode on a LEO 912 TEM fitted with an omega in-column elastic energy filter. The direct methods algorithm was then applied to merged intensities and a trial structure obtained assuming single scattering. This was further refined to obtain good agreement with a small residual of about 10% using multiple scattering calculations. A diagram of the proposed structure is given.

PACS: 61.14.Lj; 61.66.Hq; 61.14.Dc; 61.14.Lj; 61.66.Hq; 61.14.Dc

Keywords: Electron diffraction; Electron microscopy; Electron crystallography; Structure of organic crystal; Molecular structure

1. Introduction

Since the early Russian work of the 1950s [1], electron crystallography has been under continuous development as an effective method for solving the structures of difficult crystal structures, which cannot be solved by X-ray methods. The recent introduction of imaging energy filters for elastic scattering, CCD detectors, field emission guns and cold-stage goniometers, together with the increasing power of computers, has led to rapid progress in the field. For organic structures, for example, the X-ray direct methods algorithm has been successfully applied to electron diffraction data, to solve structures in many cases [2] following the first application of the method in 1976 by Dorset and Hauptman [3]. (Direct methods are numerical techniques for solving the phase problem under single scattering conditions.

*Corresponding author.
E-mail address: spence@asu.edu (J.C.H. Spence).

0304-3991/$ - see front matter © 2003 Elsevier B.V. All rights reserved.
doi:10.1016/j.ultramic.2003.08.007

The method makes assumptions of atomicity and an assumed sign for the scattering potential. It requires atomic-resolution diffraction data, and several strong reflections per atom.) Most organic crystals are extremely beam-sensitive, and are quickly destroyed under TEM imaging conditions. By contrast, electron diffraction patterns can usually be obtained from them with high resolution (better than 1 Å) using a greatly reduced electron dose. Recently, the structures of several unknown compounds including ceramic oxides [4], a new Ti–Se compound [5] and an Al_mFe precipitate in an aluminum alloy [6] have been solved using electron diffraction data. Direct methods have also been used to extend the resolution of high-resolution electron microscope images, and for solving incommensurate crystal structures [7]. They have also been used in protein crystallography [8] and for solving inorganic surface structures from surface diffraction data [9]. Other numerical algorithms, such as, maximum entropy, the log-likelihood method, and packing energy calculations [10,11] have also been developed and used in electron crystallography.

Electron diffraction patterns, unaffected by lens aberrations, induce less radiation damage than electron microscope images, and may be interpreted quantitatively for small thicknesses of organic films, especially if elastic energy filtering and a well-characterized area detector system are used [12]. For non-biological thin organic films, film bending and radiation damage appear to be the two main obstacles to obtaining reliable kinematic intensity data. In this paper, we demonstrate the use of the ''Kohler mode'' selected-area diffraction patterns, collected at low temperature from an unknown brittle hydrocarbon crystal for the determination of its structure. This new mode of diffraction provides spot diffraction patterns from much smaller areas than was possible previously. The use of low temperatures greatly reduces radiation damage, allowing collection data with improved statistics, while the use of our elastic energy filter reduces the inelastic scattering background considerably. Compared to the single-crystal X-ray diffraction method, this mode allows nano-scale crystals to be studied. The organic molecular crystals we synthesized (referred to as ''T-phase'') have quite small grain sizes and coexist with amorphous material (other reaction products) that prevented us from determining its structure by conventional single-crystal X-ray diffraction. We have therefore used an LEO 912 electron microscope with in-column elastic energy filter to collect diffraction patterns of the T-phase under low-dose conditions.

Early applications of direct methods to *n*-beam dynamical electron diffraction data showed that the method was only effective when electron diffraction patterns were taken from very thin areas, less than about 7.5 nm in thickness [13], in which case the observed intensities can be treated kinematically. In general, dynamical perturbations cannot be ignored. An interactive method, based on multislice calculations [14], as well as an empirical method combined with high-resolution microscopy [15] have been proposed to correct kinematic scattering for multiple scattering effects. In other work, dynamical effects have been included in the structure refinement using the multislice algorithm [16]. In this paper, an approximate solution (in which several atom positions are accorded high weight) is obtained initially using the kinematic approximation. The model is further improved by applying chemical constraints, taking account of the chemical bonds and molecular conformation. The model was then further refined by matching the observed dynamical diffraction intensities to the calculated ones based on the Bloch-wave method.

2. Experimental

The samples were synthesized using a new solid-state chemical reaction [17]. The initial reaction products were a mixture of amorphous material and nano-scale crystals. The size of the crystal was enlarged by annealing at 105°C for 58 h, although the amorphous matter could not be completely removed. The products were then crashed ultrasonically and then dispersed on copper grids with lacy carbon. Samples were mounted in a liquid-nitrogen double-tilt goniometer TEM holder and examined at −165°C using a LEO EM 912 electron microscope, fitted with in-column Omega

energy filter, at 120 kV. Fig. 1 shows the typical morphology of the samples. We minimized the dose using a small illumination area in the Koehler mode in order to reduce film bending. In this mode the sample is conjugate to the illumination aperture, with a demagnification of 20. By using an illumination aperture of 10 μm in diameter, this mode allows selected-area patterns to be obtained from regions as small as 500 nm in diameter. The experimental spot diffraction intensities were recorded on a cooled 14 bit $1\,K \times 1\,K$ CCD camera using a YAG single crystal scintillator as the electron detector [18]. Spot intensities were recorded using Gatan Digital Microscope software. The energy-filtered intensity within a rectangle comprising the diffraction spot was firstly accumulated as the total intensity. The background intensity was estimated as a summation of the intensity of pixels within a surrounding rectangle having the same area as the former one. The final intensity for the spot was then obtained by subtracting the background intensity from the total intensity. Unlike the X-ray case, this procedure does not produce angle-integrated data [19].

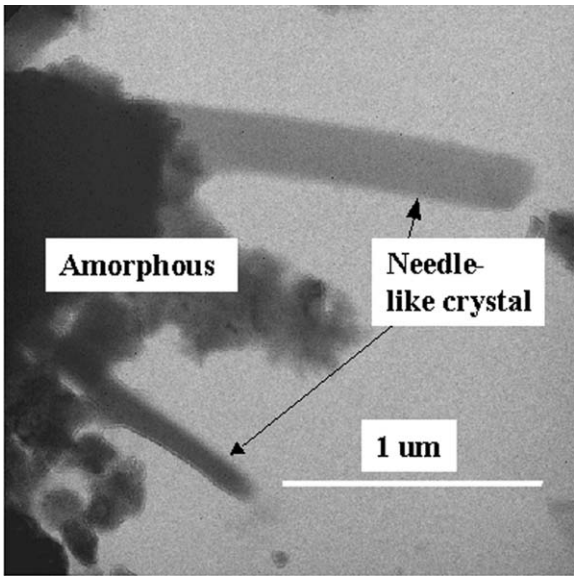

Fig. 1. Electron graph of the crystal of T-phase coexisting with amorphous phase.

3. Results and discussion

As shown in Fig. 1, the crystals are needle-like particles coexisting with the amorphous phase. The crystals' average size on the needle's side is around several hundreds of angstroms although the size along the needle direction can reach about 1 μm. We tilted the crystals in the microscope to obtain a series of nine spot diffraction patterns in order to construct a 3D reconstruction of the reciprocal lattice. The tilting axis was identified as the $[1\,0\,0]^*$ axis. Tilting in positive and negative directions from the $(0\,0\,\bar{1})^*$ plane give rise to the successive reciprocal planes $(0\,0\,\bar{1})^*$, $(0\,3\,\bar{2})^*$, $(0\,2\,\bar{1})^*$, $(0\,5\,\bar{2})^*$, $(0\,3\,\bar{1})^*$, $(0\,\bar{1}\,\bar{1})^*$, $(0\,\bar{2}\,\bar{1})^*$ and $(0\,\bar{3}\,\bar{1})^*$ with the tilting angles along $[1\,0\,0]^*$ axis of 25°, 36°, 45°, 50°, 55°, −24°, −40°, −52°. The reciprocal lattice was thus determined as triclinic lattice, with dimensions $a^* = 0.1973\,\text{Å}^{-1}$, $b^* = 0.185\,\text{Å}^{-1}$, $c^* = 0.0757\,\text{Å}^{-1}$, $\alpha^* = 83.7°$, $\beta^* = 72.4°$ and $\gamma^* = 60.4°$. The corresponding lattice parameters in real space are $a = 6.03$ Å, $b = 6.23$ Å, $c = 13.86$ Å, $\alpha = 87.26°$, $\beta = 106.69°$ and $\gamma = 119.01°$. All these tilting angles between different zones were re-calculated and found to be close to the experimental ones, verifying the correctness of the unit cell.

After finding the lattice type and unit cell, we collected more spot patterns from much thinner areas in order to reduce the influence of multiple scattering. Altogether we obtained 15 distinct diffraction patterns, which indexed as [1 0 1], [0 1 $\bar{1}$], [0 0 1], [1 $\bar{1}$ 1], [2 1 1], [2 0 1], [1 1 $\bar{2}$], [1 1 1], [0 1 $\bar{2}$], [1 2 1], [1 2 2], [2 1 2], [3 2 3], [3 2 2] and [4 $\bar{1}$ 2]. Fig. 2 shows six of them. The 3D diffraction data was normalized by equating the sum of the same indexed spots in two patterns $\sum_i I^i_{p1} = \sum_i I^i_{p2}$. Here I^i_{pn} is the observed intensity for the ith reflection in the nth spot pattern. Altogether, there were 72 independent reflections (with the highest resolution reflection of 1.002 Å). The merged intensities were evaluated initially using the kinematic approximation. The absolute scaling of intensities was obtained using the Wilson plot normalization method. The isothermal temperature factor B obtained from the Wilson plot is $4.1\,\text{Å}^{-1}$. The structure factors obtained from resulting intensities (the absolute values of the

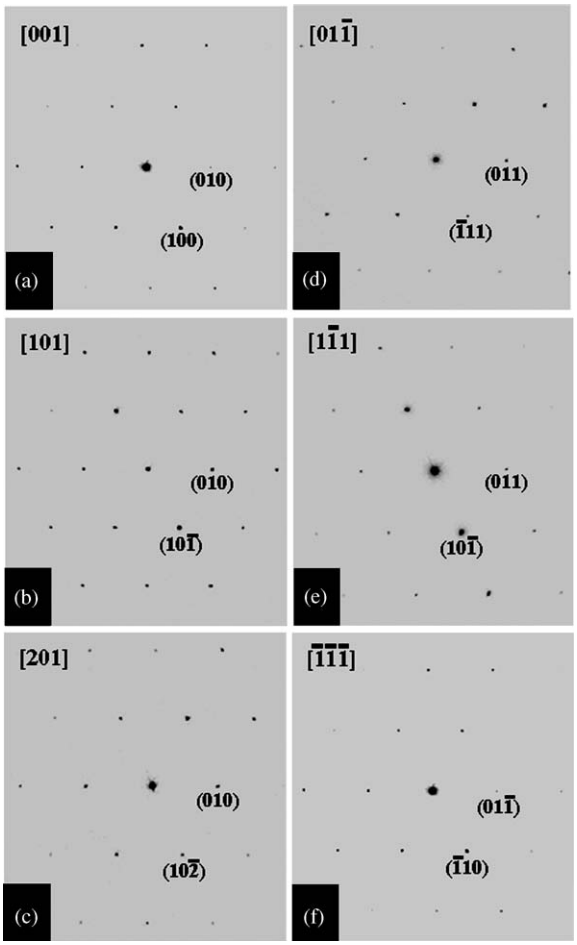

Fig. 2. Diffraction patterns of the T-phase obtained by Koehler mode at low temperature.

structure factors) were then used as input to the X-ray direct methods algorithm Shelxs [20]. At this point, we tried both the two possible space groups $P1$ and $P\bar{1}$. In general, the space group of $P1$ gave a smaller residual than $P\bar{1}$. In the following discussion, the space group has thus been set as $P1$—more accurate measurements may suggest higher symmetry. The residual R output by Shelxs was 0.245 when 33 atoms were assumed among which 12 have higher weights. The 12 atom positions with high weights were then used to form the initial trial structure.

A model structure can thus be proposed based on this trial structure, together with reasonable assumptions about the crystal chemistry. The constraints used in constructing the model include the possible molecular conformations due to required bond lengths, torsion angles and symmetry. Hydrogen positions were generated according to geometrical criteria. A structure refinement using Shelxl [20] based on this proposed model did not succeed. This is not surprising, if we note that for most of the Friedel pairs there are big differences between the intensity of $(h\,k\,l)$ and $(\bar{h}\,\bar{k}\,\bar{l})$. These could be induced by deviations of the crystal orientation from the zone axis, or by dynamical perturbations. The proposed chemically reasonable model was then refined using full dynamical calculations for the diffracted intensities. Unlike the kinematic approximation, the crystal thickness and orientation now become two new important adjustable parameters which influence the calculated intensities. Since the reflections were measured in different zones from slightly different regions of crystal, different orientation parameters and thickness may be refined for each pattern. Thus the refinement procedure was repeated for each of the six main zones. For each pattern, the orientation parameters (the reciprocal lattice vector $\boldsymbol{Kt}$, $[kt_x\,kt_y\,kt_z]$) and thickness t were treated as refinable parameters. Electron scattering factors for the atoms were taken from Peng [21]. The isotropic temperature factors for O, C and H were held constant during the refinement. As shown in the previous work [19], for hydrocarbon crystals consisting only of light atoms, dynamical effects are not so dominant as for inorganic crystals, which enables us to use structure factor matrices of relatively small dimensions. For each pattern, a structure factor matrix was constructed, whose size was determined by the number of observed reflections. We adopt here the square residual R^2 factor defined by Jansen et al. [16], which was calculated using the observed and computed intensities:

$$R^2 = \frac{\sum_i (cI_i^{\mathrm{cal}} - I_i^{\mathrm{exp}})^2}{\sum_i (I_i^{\mathrm{exp}})^2}.$$

Here I_{exp} are the experimental intensities, I_{cal} are the calculated intensities, and $c = \sum_i I_i^{\mathrm{exp}} / \sum_i I_i^{\mathrm{cal}}$ the normalization constant, $i = 1, 2, \Lambda, n$, with n the number of observed reflections in a pattern.

Table 1
For different spot patterns (column 1), R^2 factor calculated using kinematical approximation (column 6) and Bloch-wave method with the original model (column 7) and the refined model (column 8)

Zone	Thickness (nm)	Orientation			Kinematic	Bloch-wave method	
		kt_x	kt_y	kt_z		Not refined	Refined
[1 0 1]	206.2	−0.013	0.074	−0.097	0.91	0.19	0.16
[0 1 $\bar{1}$]	507.4	−0.010	−0.078	0.157	2.75	0.16	0.12
[0 0 1]	316.3	−0.083	−0.017	0.087	1.21	0.18	0.11
[1 $\bar{1}$ 1]	636.8	0.011	−0.003	−0.016	2.09	0.16	0.15
[1 1 1]	146.3	−0.028	0.019	−0.015	0.39	0.02	0.02
[2 0 1]	86.5	0.194	−0.190	−0.200	0.72	0.11	0.10

The sample thickness (column 2) and orientation (column 3–5) used in refined model are also listed.

Table 2
The coordinates of O and C atoms obtained after refinement using six electron diffraction patterns

	x	y	z
O(1)	0.5260	0.8306	0.4015
O(2)	0.8366	0.6860	0.4222
O(3)	0.8591	0.8870	0.9196
O(4)	0.1211	0.1609	0.5408
O(5)	0.5520	0.3823	0.6690
O(6)	0.8974	0.2787	0.0517
C(1)	0.2385	0.1934	0.7348
C(2)	0.4938	0.4982	0.5007
C(3)	0.7099	0.5055	0.4805
C(4)	0.2267	0.3191	0.4683
C(5)	0.6529	0.5439	0.6031
C(6)	0.0132	0.8137	0.9977
C(7)	0.2754	0.1953	0.6402
C(8)	0.9461	0.8400	0.0952
C(9)	0.0346	0.7419	0.1780
C(10)	0.9675	0.7320	0.2694
C(11)	0.8054	0.8423	0.2771
C(12)	0.0981	0.3216	0.7496
C(13)	0.7250	0.9479	0.1945
C(14)	0.7990	0.9464	0.1056
C(15)	0.0364	0.3231	0.8412
C(16)	0.0930	0.1788	0.9164
C(17)	0.2205	0.0459	0.9020
C(18)	0.2928	0.0614	0.8119
C(19)	0.0402	0.1925	0.0118
C(20)	0.7453	0.8443	0.3691
C(21)	0.3944	0.6539	0.4618

The positions of H atoms can be generated at the end of the corresponding O and C atoms by forming suitable bonds.

The refined results are listed in Table 1. When using the kinematic approximation, we see that large residuals are produced. Using Bloch-wave multiple scattering calculations, however, we find that our original trial structure shows good agreement with the data. A refinement based on the chemically reasonable model derived from this shows further improvement of R^2. We used bond lengths constrain by setting a small threshold so that the coordinates of each atom can merely have a slight change during refinement. The atomic coordinates of the atoms obtained from the refinement are listed in Table 2, and a diagram of the structure is given in Fig. 3. In the final structure model, the shortest bond of C–O is 1.36 Å (O5 and C5) and that of C–C is 1.38 Å (C8 and C14). Although electron diffraction showed great advantages in studying the structure of tiny crystal of T-phase, the construction of the chemically reasonable model was also critical. Electron diffraction combined with other physical or non-physical means in structural analysis is more useful.

4. Conclusion

Using electron diffraction and direct methods we have obtained a space group, cell constants and some initial atomic position parameters for nanocrystals of a new hydrocarbon T-phase by energy-filtered electron diffraction in the Koehler mode. A chemically reasonable model of the crystal was then derived based on a careful examination of the molecular conformation and our initial model. This model was further refined using Bloch-wave multiple scattering calculations, to produce an

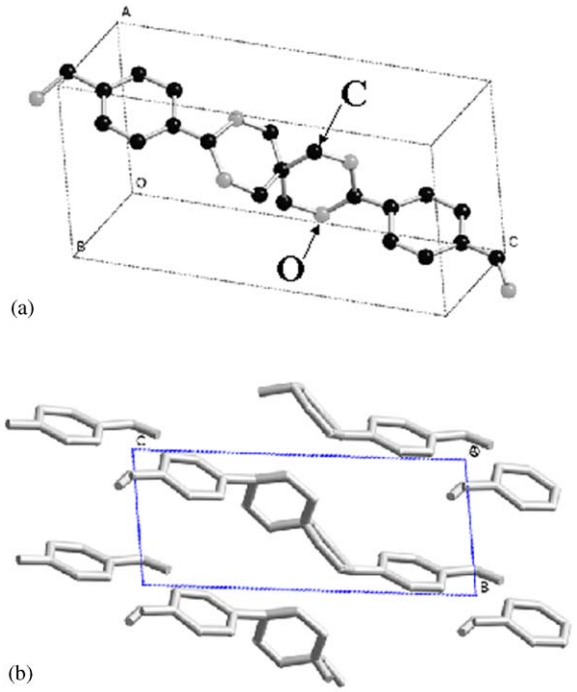

Fig. 3. (a) Illustration of a molecule in the unit cell and (b) stacking of molecules of the structure. The O, C and H atoms are indicated in (a).

excellent fit between the experimental and calculated intensities.

Acknowledgements

This work is supported by ARO award DAAD190010500.

References

[1] B. Vainshtein, Structure Analysis by Electron Diffraction, Pergamon Press, London, 1964.
[2] D.L. Dorset, Structural Electron Crystallography, Plenum Press, New York, 1995.
[3] D.L. Dorset, H.A. Hauptman, Ultramicroscopy 1 (1976) 195.
[4] W. Sinkler, E. Bengu, L.D. Marks, Acta Crystallogr. A 54 (1998) 591.
[5] T.E. Weirich, X.D. Zou, R. Ramlau, A. Simon, G.L. Cascarano, C. Giacovazzo, S. Hovmoller, Acta Crystallogr. A 56 (2000) 29.
[6] J. Gjønnes, V. Hansen, B.S. Berg, P. Runde, Y.F. Cheng, K. Gjønnes, D.L. Dorset, C.J. Gilmore, Acta Crystallogr. A 54 (1998) 306.
[7] H.F. Fan, Microsc. Res. Tech. 46 (1999) 104.
[8] D.L. Dorset, C.J. Gilmore, Acta Crystallogr. A 55 (1999) 448.
[9] C.J. Gilmore, L.D. Marks, D. Grozea, C. Collazo, E. Landree, R.D. Twesten, Surf. Sci. 381 (1997) 77.
[10] I.G. Voigt-Martin, H. Kothe, A.V. Yakimansky, A.V. Tenkovtsev, H. Zandbergen, J. Jansen, C. Gilmore, Ultramicroscopy 83 (2000) 33.
[11] R.C. Yu, A.V. Yakimansky, H. Kothe, I.G. Voigt-Martin, D. Schollmeyer, J. Jansen, H. Zandbergen, A.V. Tenkovtsev, Acta Crystallogr. A 56 (2000) 436.
[12] J.M. Zuo, Microsc. Res. Tech. 49 (2000) 245.
[13] D.L. Dorset, B.K. Jap, M.-Hs. Ho, R.M. Glaeser, Acta Crystallogr. A 35 (1979) 1001.
[14] B.D. Sha, H.F. Fan, F.H. Li, Acta Crystallogr. A 49 (1993) 877.
[15] D.X. Huang, W. Liu, Y.X. Gu, J.W. Xiong, H.F. Fan, F.H. Li, Acta Crystallogr. A 52 (1996) 152.
[16] J. Jansen, D. Tang, H.W. Zandbergen, H. Schenk, Acta Crystallogr. A 54 (1998) 91.
[17] N. Melcer, O.M. Yaghi, 2003, in preparation.
[18] J.C.H. Spence, J.M. Zuo, Rev. Sci. Instrum. 59 (1988) 2102.
[19] J.S. Wu, J.C.H. Spence, Acta Crystallogr. A 58 (2002) 580.
[20] G.M. Sheldrick, Acta Crystallogr. A 46 (1990) 467.
[21] L.M. Peng, Micron 30 (1999) 625.